

Numerical investigation on the volute cutwater for pumps running in turbine mode

Alessandro Morabito ^{a,*}, Elena Vagnoni ^b, Mariano Di Matteo ^a, Patrick Hendrick ^{a, **}

^a Aero-Thermo-Mechanics Department, Université Libre de Bruxelles - ULB, Brussels, Belgium

^b Laboratory for Hydraulic Machines, École Polytechnique Fédérale de Lausanne - EPFL, Lausanne, Switzerland



ARTICLE INFO

Article history:

Received 3 December 2020

Received in revised form

22 March 2021

Accepted 21 April 2021

Available online 3 May 2021

Keywords:

Pump as turbine

Computational fluid dynamic

Optimization

Hydraulic efficiency

ABSTRACT

The hydropower sector has recently raised the interest in pump as turbine (PaT) that can be a valid trade-off between capital cost and performance in micro-scale installations. Nevertheless, the modest efficiency of PaTs often restricts their exploitation. In this paper, available experimental data are used to tune a numerical model which aims to investigate the effect of the pump cutwater design on the PaT performance to improve the hydraulic efficiency. Because of its finite thickness, the cutwater interferes with the flow at the runner inlet, and generates local flaws in the velocity field such as swirl and deviations of the streamlines which limit the machine performance. To identify the geometrical characteristics of the cutwater impacting on the PaT performances, different values of stretching and thickness of the cutwater are studied at variable inclination by computational fluid dynamics (CFD) simulations. A multivariate regression method is applied on the CFD results to build a surrogate model of the PaT hydraulic characteristics as a function of the geometrical parameters of the machine cutwater. Based on this model, an optimization problem is solved to identify the most advantageous geometrical asset of the PaT cutwater to maximize the efficiency. The results highlight that the length and the cutwater angle are the most affecting variables in favouring a tangential component at the entrance of the runner. The hydraulic efficiency peak of the optimized geometry results to be 86.3%, while the baseline configuration records an efficiency of 82.4%, and the $\Psi - \phi$ characteristic moves the best efficiency point towards higher head (+7.5%) and lower discharge (−13.0%). The proposed methodology allows identifying the best geometrical characteristics of the PaT cutwater to maximize the performances while significantly reducing the computational time.

© 2021 Elsevier Ltd. All rights reserved.

1. Introduction

The growing consciousness of the need for a green alternative to other pollutant energy sources has enhanced the spreading and integration of renewable energy sources [1]. Solar and wind energy sources have recorded the highest growth in the last decades, nevertheless, today, hydropower represents the largest share of renewable energy sources in the world [2]. It can be exploited by natural or artificial water sources [3–5] and its implementation is present in different scale sizes [6–8]. Among several components of a hydropower plant, the hydroelectric unit is the very heart of the energy production system and thus its performance is crucial for

the return on investment of the power plant [9]. The selection of the right type of turbine for given site conditions is one of the most relevant factors influencing operational costs and revenues; hydraulic turbines have high costs due to their punctual design and performance testing [10]. Electromechanical elements represent between the 20–35% of the total investment [11], but it can reach higher values (70%) in certain projects, where civil engineering costs are reduced by pre-existing infrastructures on-site [10,11]. However, in micro-scales hydropower projects, the initial capital investment of a conventional hydroelectric unit is hard to be determined and often economically prohibitive [12].

An effective method to shorten the costs in turbomachinery in

* Corresponding author.

** Corresponding author.

E-mail addresses: alessandro.morabito@ulb.be (A. Morabito), patrick.hendrick@ulb.be (P. Hendrick).

the micro-scale hydropower is the implementation of centrifugal or diagonal pumps in reverse mode (opposite flow direction and rotational speed than normal operation) instead of conventional turbines. The major benefit in using pumps as turbine (PaT) is that pumps are comparatively much more cost-effective than conventional hydraulic turbines [10,11,13]. Pumps are mass-produced and have low initial and maintenance costs but ready availability [14]. The exploitation of micro- and mini-scales hydropower finds in PaT a strong ally for the rural and remote decentralized applications [15–17]: PaTs are relatively simple, and their solid structure provides a reliable option for renewable energy provision. However, PaTs have a drawback concerning the performance prediction method, as there is no universal model of conversion from the normal pump operation [10,18,19]. Many researchers have proposed analytical and experimental models in forecasting the stability and the best efficiency point (BEP) of a pump in reverse mode [20–22]. However, the diversity of the experimental results and consequent difficulties in the validation of the developed predictive models [11,23,24] continue to motivate world-class research activities in this field, being of high interest for industry and academics in micro-hydropower [25,26] and energy recovery instead of throttling [27].

Furthermore, pumps for industrial applications are not meant to run in reverse mode and their performance can shift appreciably from the higher efficiency of traditional hydraulic turbines. Many attempts have been studied and engineered to bring performance improvements in using PaTs. The study on coupling the effect of adjustable guide vanes (AGV) to an axial pump allowed Qian et al. [28] to generate a hill chart also in reverse mode and extend the PaT operating range at high efficiency. This technology takes advantage of the variable guide vanes pitch to compose the most suitable velocity triangle at the inlet of the runner. On this topic, another experimental investigation shows the positive effect of a volute equipped with guide vanes for flow regulation [12]. The act of providing inlet flow control can guarantee the PaT to operate efficiently at off-design conditions, that could often happen in micro and mini hydropower system for the limited capacity of the water reservoir or during seasonal fluctuations of the water availability [12,29]. However, common water pumps are not equipped with guide vanes and even less often with AGV. This additional feature affects the final cost of the pump and compromises the economic strength of PaTs unless to accommodate variable hydrological load conditions.

Several efforts have been done to improve the impeller geometry. A parametric optimization of single-curvature blade profile of a PaT was carried out by combining the back propagation neural network and genetic algorithm: under the BEP condition, the efficiency of the PaT increased by 2.91% after optimization [30]. Efficiency impeller improvements for PaT operation have been presented by Derakhshan et al. [31] by using a gradient-based optimization CAD-connected and supported by CFD validation. The new blade design results performing at about +3% better than the initial pump design and slightly reduced head and torque (−3% and −7% respectively) [31]. Machine learning techniques, like regression models, have been applied to improve the design of an impeller for off-design and nominal working conditions by developing a multi-objective optimization problem [32]. Wang et al. [33] conducted a numerical and experimental analysis of three new special forward-curve impellers. Although the efficiency improvements are obtained, the impeller replacement represents an expensive re-design of the machinery. A less intensive geometrical modification has been experimentally conducted on the rounding of the pump outlet edges of impeller blades, namely the PaT runner inlet. This operation mitigates the water shock at the inlet of the same pump in reverse mode and reduces the hydraulic losses

through the blade channels [34]. The effect of the blade thickness on the PaT efficiency is proven by a throughout analysis of the hydraulic loss distribution in three different pumps which indicates that the total hydraulic loss in a PaT increases with the blade thickness [35]. Further experimental investigations have been performed on other modifications of the impeller geometry by the impeller trimming [36], impeller diameter size [37,38], rotational speed [38], blade wrap angle [39] and, again, impeller edges rounding [31,40,41]. Moreover, the behaviour of several hydraulic components have been studied in a comprehensive investigation at BEP, part-load, and full load conditions to evaluate four different geometrical modifications in eight PaTs [42]: the inlet impeller rounding and inlet casing rings have been improved to increase the efficiency, while the modification of the pump suction eye enlargement and the casing eye-rib removal have shown a mingled effect on the performance [42,43]. Additional theoretical and numerical analysis are present in the literature for the use of splitter blades in PaT: CFD steady-state simulations were found in good agreement with experimental results although a numerical overestimation of the efficiency due to hydraulic neglected losses [44]. Capurso et al. develop a novel impeller design for low-medium specific speed double suction centrifugal pump [45] and analysed in reverse mode [46]. The novel double suction impeller is characterized by a new arrangement of its flow channels, which come up alternately on the same circumferential exit. Numerical analysis supports the performance assessment of new channel arrangement for guiding the flow at the inlet of the PaT runner in absence of a diffuser [46]. Also, a numerical analysis has shown by steady-state simulations the presence of an optimum in the PaT overall performance of the three pumps analysed by the effect of the radial gap at the rotor/stator interface [47]. Finally, new designs of the volute casing have been numerically analysed to reduce radial forces affecting the pump normal and reverse operation [48]: the novel casing design provides a more sustainable mechanical operating conditions, allowing the PaT to run with competitive hydraulic efficiency. Recently, the same research group of the University of Tehran demonstrates the implication of the cutwater for a low-specific speed pump performance by an experimental study over the pressure fluctuation in the rotor/stator interaction [49]. Interestingly, the correct positioning of the cutwater appears to be beneficial in increasing the momentum at the inlet of the PaT runner.

Previous research investigations in the PaTs performance underline the growing interest in improving its efficiency and promoting their implementation in micro hydropower. However, drastic geometrical updates would not preserve the PaTs economic advantage, but they may require a considerable amount of resources instead. On the contrary, cutwater modifications are confined in a modest area of the volute and do not alter the runner geometry. Because of its finite thickness, the cutwater interferes with the flow, generating local excess velocities and deviations of the streamlines affecting the flow orientation at the inlet of the PaT runner and consequently its performance. Thanks to the few preliminary study about the effect of the cutwater, it has been possible to foresee its design potential in pumps in reversed mode, but the precedent literature concerning an effective methodology in its design optimization is limited.

The objective of this article is to present a new approach for a geometry improvement based on numerical investigations. The produced data allow building a regression model of the PaT efficiency and to detect with good accuracy the geometry optimum for the new cutwater design thanks to the solution of an optimization problem. The analysis is conducted on the variations of the rounding, length and angle inclination of the volute cutwater of a radial-pump. For this purpose, Section 2 announces the problem

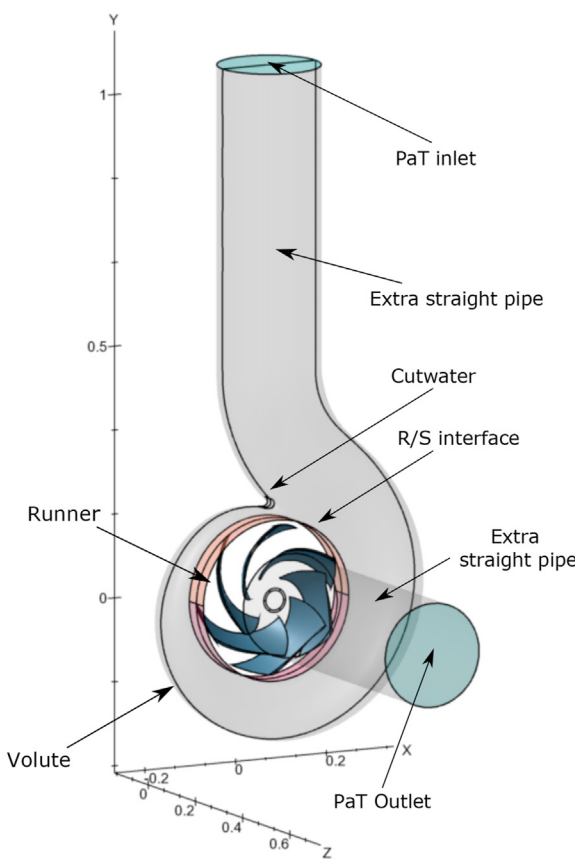


Fig. 1. Overview of the simulated domain. Dimensions are expressed in meters.

statements and introduces the developed methodology. Section 3 firstly illustrates the hydraulic domains, giving a view of the phenomenological problem driven by the cutwater modifications. The numerical approach and the available experimental data are then discussed. Finally, the regression model and the optimization strategy are presented. The CFD validation and results are described in Section 4 and they address to the finding of the cutwater optimum design. The proposed numerical investigation offers sufficient pool of data to elaborate a predictive algorithm of the hydraulic PaT

performance. The optimized geometry of the cutwater is proposed and compared with its baseline design. At last, the conclusions are stated in Section 5.

2. Problem statement

To optimize a centrifugal pump running as a turbine, the present study aims at investigating the cutwater geometrical parameters, under predefined constraints, that maximize the hydraulic efficiency. An overview of the investigated geometry is given by Fig. 1. The cutwater is modified from its initial design (baseline geometry) by length, tip thickness and tilt deviation. The geometrical updates are conducted on case-by-case basis by a computer-aided design (CAD) software and adapted for numerical simulations. To secure reliability of the selected numerical model, the computational results of the baseline geometry are validated by experimental measurements in respect of their relative accuracy. Therefore, CFD simulations build a complete data-set, including the PaT head and efficiency characteristics. The retrieved data allow the development of a regression model for understanding the effect of the different geometrical variables on the hydraulic efficiency. Moreover, this model is able to predict the PaT performance in relation of the cutwater design and lessen the investigation time appreciably. Finally, an optimization problem, targeting the highest efficiency point, processes the regression model and converged in an ultimate optimal design of the cutwater.

3. Methodology

3.1. Hydraulic domain modelling

To reproduce the operating domains of the pump, its technical drawing, provided by the manufacturer, have been imported in CATIA V5 and healed by geometrical imperfections, such as disconnected surfaces and missing intersecting points. A dedicated smoothing-CAD process is applied to the investigated sub-domains in order to emulate fine and smooth surfaces nearabout the cutwater (Fig. 2). In this way, erroneous sharp edges and inaccurate defects are removed from the domain modelling, saving critical geometrical spots, such as bulges and cusps, to the mesh generation process and numerical computations. The domain implemented for the generation of the computational grid counts four sub-domains: the pump impeller, the volute and two straight pipes at the suction and discharge side of the pump (Fig. 1). The additional volumes are meant to uniform the imposition of the boundary condition during

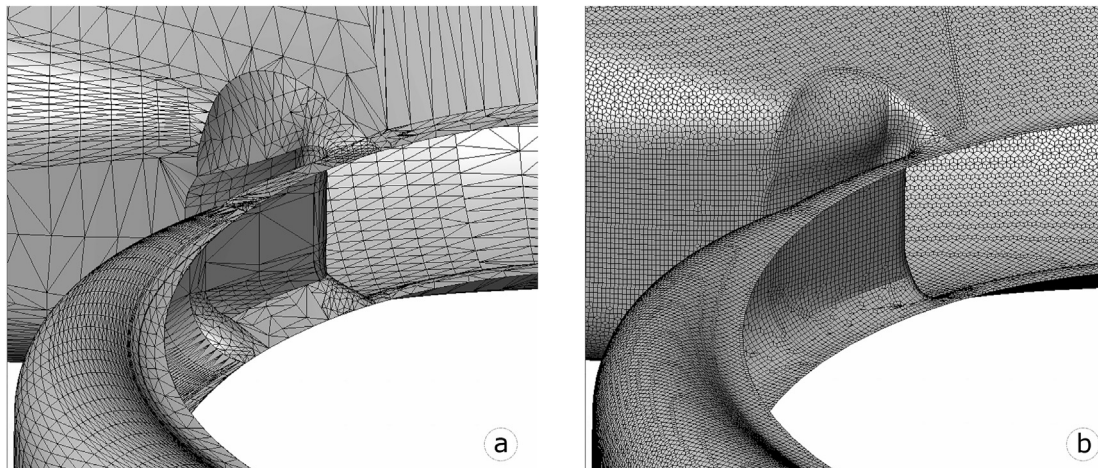


Fig. 2. Domain geometry improvements by rebuilding the cutwater's adjacent surfaces for its stretched version: (a) before and (b) after the geometrical improvements.

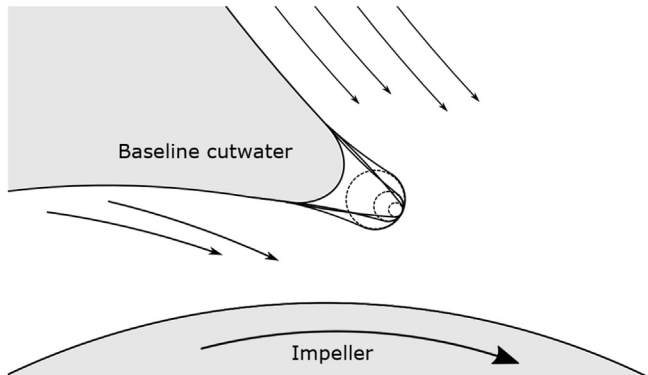


Fig. 3. Variation of the cutwater rounding.

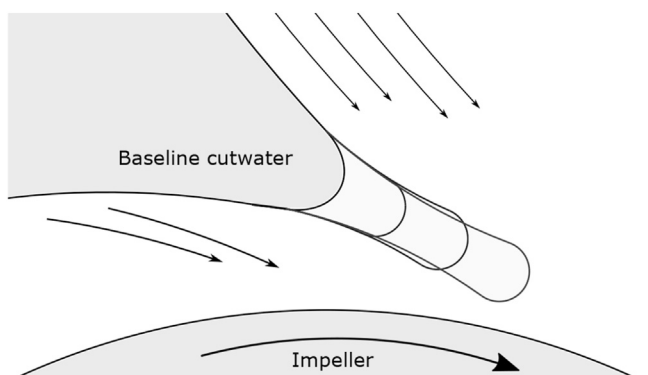


Fig. 4. Variation of the cutwater length.

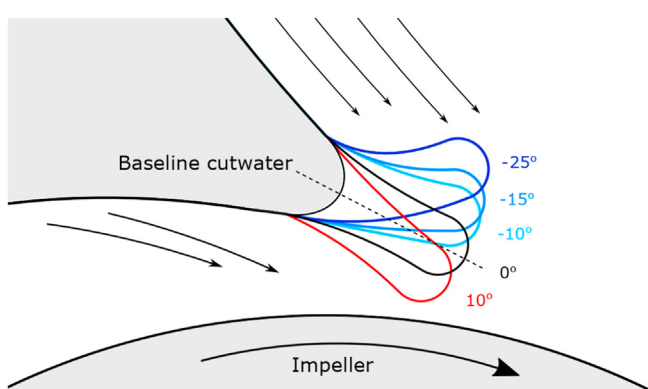


Fig. 5. Variation of the cutwater tilt angle.

Table 1
List of independent variables describing the cutwater.

Variable	Domain
Stretching, S	$\Delta_S = [L, 4L]$
Rounding, R	$\Delta_R = [r/4, r]$
Angle, A	$\Delta_A = [-25^\circ, +10^\circ]$
Discharge unit, Q_{11}	$\Delta_{Q_{11}} = [0.33, 0.50]$
Speed unit, n_{11}	$\Delta_{n_{11}} = [65, 105]$

the solver calculations without affecting the solution of the simulation [50]. Despite the increase of simulated flow and thus the larger use of computational resources, both sub-domains allow the flow to reach the full developed conditions and avoid severing the

computation right at the interested research sections.

In this research, the modifications of the cutwater's length, thickness and tilt angle report to the baseline design of the volute. The original dimensions are denoted by the length of 15,6 mm (L) and a thickness for 6,5 mm of radius (r). The inclination angle of the original cutwater is set to 0° . The limits of proposed modifications reflect geometrical constraints. The maximum inclination is defined to avoid the contact with the rotor and the minimum thickness and length by structural and manufacturing issue. The investigation analyses the cutwater's radius at full, half and quarter of the baseline size (Fig. 3). The effects of cutwater's length are covered by CFD simulations on multiple sample stretching values i.e. two, three and four times the baseline length (Fig. 4). Finally, the inclination of the cutwater represents an additional optimization parameter: cutwater with positive and negative angle deviations are explored (Fig. 5).

The modifications performed on the cutwater geometry are investigated within the ranges summarised in Table 1 and the research space covers the operative intervals of Q_{11} and n_{11} where high efficiency is performed. Q_{11} and n_{11} are defined as follows in Eq. (1):

$$\begin{aligned} Q_{11} &= \frac{Q}{D^2 H^{0.5}} \\ n_{11} &= \frac{nD}{H^{0.5}} \end{aligned} \quad (1)$$

The investigated geometry alterations would affect the flow pattern at the entrance of the PaT runner such as the absolute water speed c_2 direction, α_2 . The hydraulic performance of the PaT depends on the specific energy, which increases through the turbo-machine according to Eq. (2) [51]:

$$\begin{aligned} E &= gH \\ &= u_2 c_{2u} - u_1 c_{1u} \\ &= u_2 c_{2m} \cot(\alpha_2) - u_1^2 + u_1 c_{m1} \cot(\beta_1) \end{aligned} \quad (2)$$

An overview of the nomenclature and the velocity triangles in pump running in turbine mode is provided by Fig. 6.

3.2. Mesh generation

The domain discretization are generated separately for the sub-domains by utilizing commercial CFD codes from Numeca. Auto-Grid5™ software [52] produces a structured mesh of a single passage of the six-blade-runner. The solver will then implement the full periodicity of the runner blade passages for achieving the numerical results. Hexpress [53] and Hexpress-hybrid [54] are used for the unstructured mesh of the other sub-domains and the final merged mesh. All the available experienced numerical simulations confirm the relevance of the grid quality as a crucial factor for convergence and simulation reliability [32,50]. For this purpose, a grid sensitivity analysis is conducted with an increasing number of mesh points and improved quality (Fig. 7), in respect of the maximum level of orthogonality (average skewness $> 75^\circ$), average expansion ratio ($\bar{ER} < 5$), acceptable ER at viscous layer ($ER \leq 1.2$) and average aspect ratio ($\bar{AR} \leq 5$). The final mesh is considered acceptable when the generated outputs do not show great sensitivity to local or global grid refinements [49,55]. The convergence criterion is set at 10^{-4} and, until the converged values for efficiency and torque exceed the range of 0.04% from the solution obtained with a finer mesh, the number of the grid points are further increased. Table 2 illustrates the details of the mesh in the four sub-domains used for the baseline case study. \bar{ER} and \bar{AR} give an index of the mesh quality and dx estimates the average element size,

calculated as $dx = (V/n_{nd})^{1/3}$, where V is the domain volume [m^3] and n_{nd} is the number of mesh nodes.

The non-dimensional wall distance y_+ defines the requirements for a sufficient and accurate description of the turbulence at the wall. Hence, it is crucial to monitor that y_+ ranges in the admissible values in solving the boundary layer. An iterative adjustment of the first-cell size, according to the adopted turbulent model, and grid refinement are conducted to find the adequate set of mesh for different discharge regimes. The shift in flow velocities affects the Reynolds number, and thus, the approach in estimating the boundary layer. The y_+ values reported in Fig. 8 are representative for all the investigated cases and simulated discharge values. A whole mesh system of the four sub-domains between $4.8 \cdot 10^6$ and $6 \cdot 10^6$ cells is found satisfactory. The cells number variation is mostly due to the turbulence model selection and the additional refinements near to cutwater during its modifications: the wider the inclination angle and length, the larger the required number of grid cells.

3.3. Numerical modelling

The selection of a suitable turbulence model is of crucial importance for the significance of the simulations. Six different models have been tested to solve the incompressible Reynolds time-averaged Navier-Stokes (RANS) equations. The simulations run in steady-state and aim to look at the design validity of the cutwater, describing the flow field perturbations in the volute and velocity angles at the inlet of the runner. Thoroughly solving the relative motion between rotor and volute requires an unsteady and viscous flow solver with the capacity to manage enormous data storage. One way to optimize the calculation requirement is to resolve the steady flow field on a truncated computational domain. This requires the so-called mixing plane approach, an averaging process to be performed at the rotor/stator (R/S) interfaces [56]. In this condition, the PaT cutwater does not locally influence the inlet of the runner but the circumferential averaged flow quantities are exchanged at R/S interfaces. However, the resultant simulation is still capable of predicting with reasonable accuracy the blade-to-blade flow-field and the rotor and stator's overall performance [56,57]. This physical approximation tends to become more

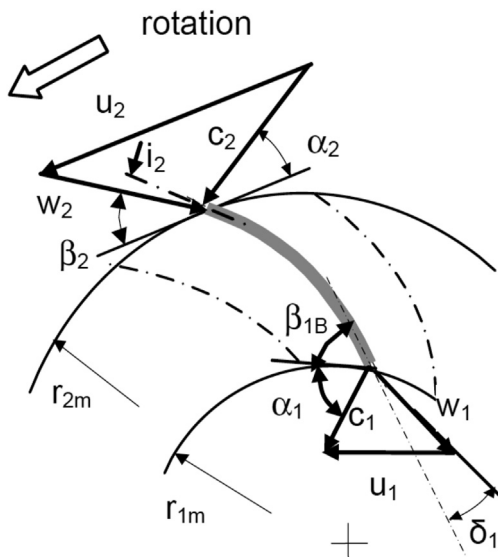


Fig. 6. Velocity triangles at the entrance (station 2) and exit (station 1) of the PaT runner [51].

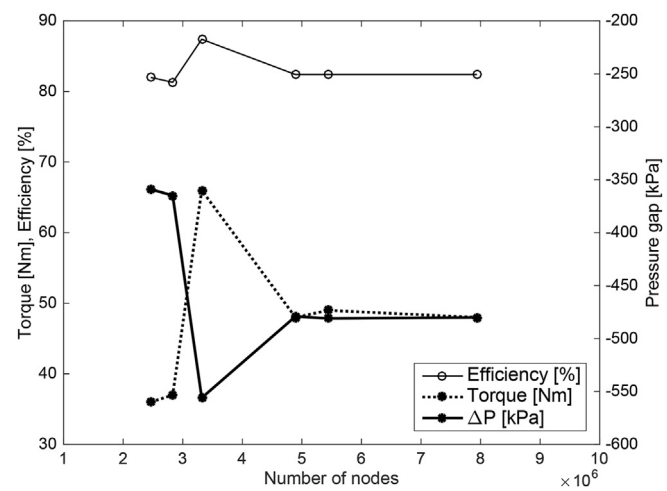


Fig. 7. Mesh convergence test conducted to assess the independence of the grid on the accuracy of the solution.

Table 2

Mesh details for the baseline case study domain.

Sub-domain	Volume [m^3]	Nodes	$dx [\text{m}]$	\bar{AR}	\bar{ER}
Inlet	0.0198	450 953	0.0035	1.01	1.16
Volute	0.0247	2 791 970	0.0021	1.01	1.10
Blade	0.0095	1 190 496	0.0019	1.72	1.25
Outlet	0.0201	460 359	0.0035	1.01	1.16

acceptable as the rotational speed is increased [56]. Finally, the mixing plane approach decreases the needed computational effort by up to an order of magnitude compared to unsteady simulations, that is too time-consuming for use in routine design [58,59] because it requires different definitions of the spatial and temporal scales of the problem. In this research investigation, a mixing plane approach is implemented with a full non-matching technique that allows for not congruent topology of mesh patches on both sides of the R/S interfaces.

In agreement with other numerical investigation on internal flow with relevant pressure gradient [48,60,61], $k-\omega$ SST better reproduces the revised characteristic curves of the pump and PaT. This turbulence model is used for all the simulations presented in this investigation. Table 3 represents an extraction of the aforementioned turbulence model test over a mesh in a range of 3.9–4.6 million nodes. This grid difference is due to the different approach to resolve the boundary layers for extended wall function (EWF) and standards model. In EWF treatments, each wall-adjacent cell's centroid should be located within the log-law layer, $30 < y_+ < 300$ requires a greater first cell height, thus, a reduced total number of nodes than a standard model ($y_+ \approx 1$).

The numerical discretization scheme is set central and of the second order. The simulations are computed in FINE/Open solver [56] and for smoothing the calculations, multigrid initialisation is employed: multiple levels of initial coarser grids are used to prepare the computation with the finest grade. A no-slip boundary condition is applied to all the internal wall. The mass flow direction is set normal to the inlet surface and static pressure constant value at the outlet. The numerical settings for the pump mode are similar to the PaT mode but with switched inlet and outlet sections and opposite direction of the rotational speed. Indeed, in the micro pumped hydro energy storage (PHES) system where the PaT operates, the machine is able to operate both in generating and

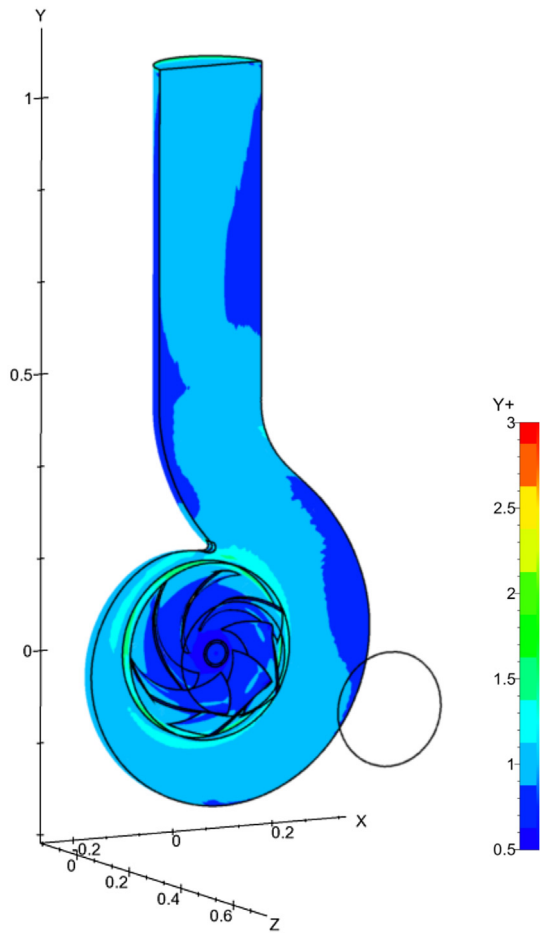


Fig. 8. Evaluation of non-dimensional wall distance y^+ for the volute and impeller in the baseline case.

pumping modes and the BEPs are found at -700 rpm and 1000 rpm, respectively [62]. The performance of the turbomachine and the cutwater influence are analysed for a series of discharge values. The time required to obtain converged results is on average above four and a half hours (with 12 cores parallel calculations). The convergence criterion is not defined unequivocally by examining the residuals but also from the imbalance of mass and momentum and stable outputs.

3.4. Experimental setup

In this study, experimental tests are used to validate the numerical simulations performed on the centrifugal pump. The pump

Table 3

Turbulent model test applied to a PaT: Spalart-Allmaras (SA), k- ϵ models, k- ω with or without Extended Wall Function (EWF).

Model	PaT mode at N_{PAT}		
	ΔP [kPa]	M [Nm]	η_h [%]
SA	-455	-45.9	82.2
SA EWF	-451	-45.9	82.8
k- ϵ Yang Shih	-525	-57.1	83.0
k- ϵ EWF	-525	-56.0	83.4
k- ω SST	-479	-48.0	82.4
k- ω SST EWF	-525	-53.4	82.8
Experimental data	-492	-49.0	78.2

specific speed N_s , a designing value that helps to characterize the shape of the impeller pump, is equal to 55 and it is calculated as follows in Eq. (3):

$$N_s = \frac{N\sqrt{Q}}{(H)^{0.75}} \quad (3)$$

where N [rpm], Q [m^3/s], and H [m] are related to the pump BEP. The radial pump is applied in a 7 kW micro pumped storage plant facility generating 17 kWh in the industrial suburb of Froyennes, in Belgium [62]. In this installation, the pump without any modifications is used for both pumping and generating operations by variable speed control. The main parameters of the pump are listed in Table 4 and details of the geometry are shown by Fig. 9.

Data is acquired in steady state operations with a frequency of 1 Hz by sensors placed in key sections of the facility line, as represented in Fig. 10. Pressure and temperature are measured upstream and downstream the turbomachine. The flow-meter is installed on the straight pipe at the convenient distance and the pump shaft is equipped with a torque-meter for monitoring the couple and rotational velocity. The experimental results are averaged values over a total number of 300 samples per steady operating condition. The precision of a given single parameter is computed with the uncertainty model expressed in Eq. (4):

$$U = \pm \left[(B_{err})^2 + (t_{95} S_{\bar{X},err})^2 \right]^{1/2} \quad (4)$$

where U is the uncertainty of the parameter, B_{err} is the systematic error (or bias error), $S_{\bar{X},err}$ is the precision index error (or random error), and t_{95} is the Student's t degree of freedom and is computed with the Welch-Satterthwaite approximation [63]. The precision index error in Eq. (5) is determined by the square root of the sum of the square random uncertainties $S_{\bar{X}_i}$:

$$S_{\bar{X},err} = \sqrt{\sum_{i=1}^K \left(S_{\bar{X}_i} \right)^2} \quad (5)$$

The $S_{\bar{X}_i}$ is the standard deviation divided by the square root of the number of samples for the i^{th} element. The high number of samples acquired in these tests reduces $S_{\bar{X},err}$ making it negligible. Therefore, only the systematic error, that remain constant in the whole test [64], is taken in consideration. It is calculated in Eq. (6) by the square root sum of the square of the single systematic error B_i :

Table 4

Extract of the main parameters data-sheet of the pump installed at the micro pumped storage facility.

Pump main parameters	
Installation year	2017
Horizontal axis	
PaT BEP rotational speed, N_{PaT}	-700 min $^{-1}$
Diameter suction side	250 mm
Diameter discharge side	200 mm
Number of blades	6
Blade thickness at exit	2.8 mm
Blade thickness at mid-channel	5.2 mm
Specific speed	55
Impeller exit diameter	296 mm
Impeller exit width	45.6 mm
λ hub	33°
λ shroud	31°
β_2 hub	33.6°
β_2 shroud	31.5°

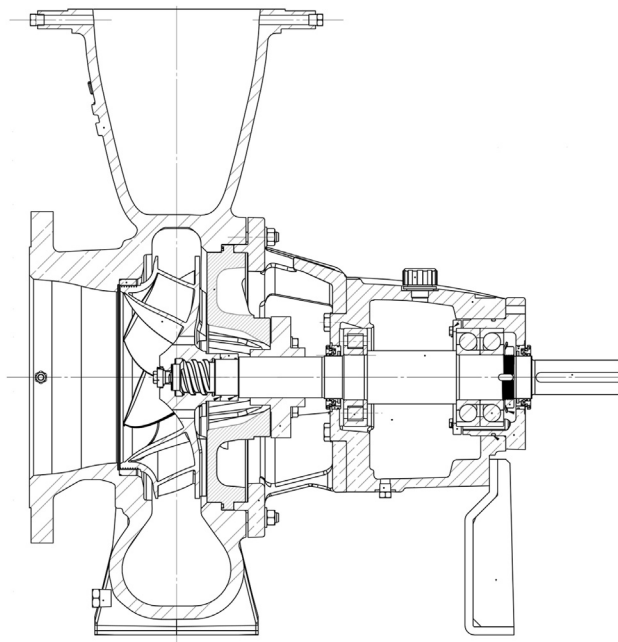


Fig. 9. Sectional view of the PaT.

$$B_{err} = \sqrt{\sum_{i=1}^K B_i^2} \quad (6)$$

The error measured for each parameter propagates in derived results through the following propagation relationship of Eq. (7):

$$\frac{\partial f}{f} = \sqrt{\left(\frac{\partial f_1}{f_1}\right)^2 + \dots + \left(\frac{\partial f_k}{f_k}\right)^2} \quad (7)$$

in which $f = f(f_i)$ is the combined results, ∂f is the associated uncertainty of the quantity f , while ∂f_i are the uncertainty of the independent parameters f_i . The bias and the random error should be taken in consideration separately until summed as seen in Eq. (4), but since we consider the random error negligible only the bias error will be considered for the error propagation.

Fig. 11 shows the propagation of the relative error for the different parameters measured and the derived system efficiency, expressed as $\eta = M\omega/\rho g Q H$, in function of the discharge number $\phi = Q/\pi\omega D^3$.

3.5. Multivariate regression model

Relying on the data-set produced by the simulated operating points, a surrogate model of the PaT performances is built by employing the multivariate adaptive regression spline method (MARS) [65]. The MARS algorithm is a non-parametric multivariate regression method that approximates a nonlinear correlation by a series of spline functions on different intervals of the independent variable. The sequence of these spline functions is articulated by recursive partitioning, or hinge functions, which includes branched equation modelling and assures the continuity of the resulting analytical function and of its first derivative. Hinge mapping of the developed MARS model can be expressed as in Eq. (8):

$$BF_i = h_i * \text{Max}[0, (x_j - K)] \quad (8)$$

where i and j are the indices for basis functions (BF) and input variables (x), respectively, and K is a constant referred as knot. The $(x - K)$ condition greater than zero enables the related function factor, h . In this way, MARS builds regression based surrogate models by adding BFs as a mechanism that defines variable intervals severed by knots. Once the full set of basis functions combinations has been created, the algorithm sequentially removes individual basis functions that do not significantly contribute to the model equation [66]. In the backward-pass process of the MARS implementation several BFs are discarded from the final model expression as not significant or held in more influencing hinge

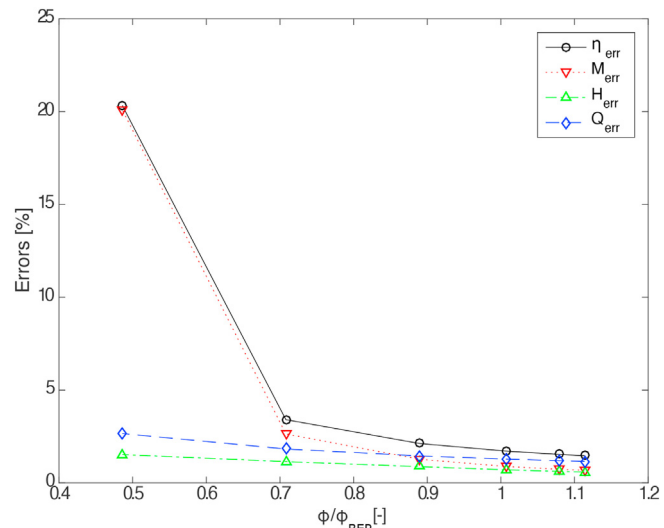


Fig. 11. Error propagation in function of the dimensionless discharge number.

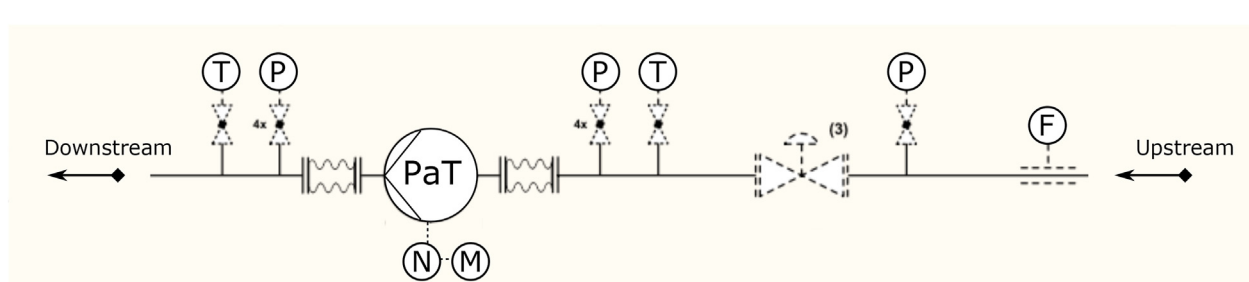


Fig. 10. Schematic view of the micro-hydropower station and location of the measurement devices: \circledcirc pressure sensors, \circledast thermo-couples, \circledcirc tachometer, \circledcirc torque-meter, \circledcirc flow-meter.

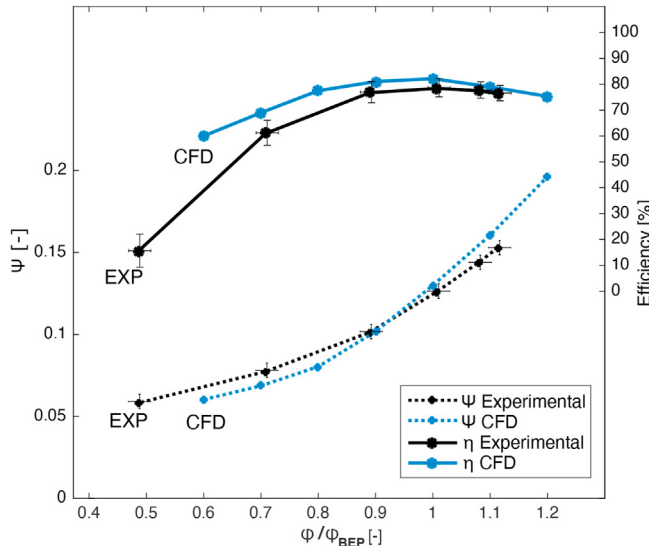


Fig. 12. Numerical and experimental comparison for specific energy coefficient Ψ and efficiency η_h over the relative discharge number.

functions [66]. For this reason, some of the BFs are pruned in the final formulation of the surrogate model.

The target of the model is to compute a formulation of the predicted PaT efficiency, $\hat{\eta}$, by the investigated variable ranges, as previously listed in Table 1. $\hat{\eta}$ is given by a function dependent on the operating conditions (Q_{11} and n_{11}) and the geometrical variables (S, R, A) that define the modification of the cutwater. In addition, in order to set consistency of the $\hat{\eta}$ formulation with the feasible PaT working conditions, an admissible design space of the Q_{11} - n_{11} relation needs to be resolved. Therefore, an analytical function $\hat{Q}_{11} = g(S, R, A, n_{11})$ is established by applying the MARS method to the available numerical data. Because of this second correlation of Q_{11} , the model of the PaT efficiency also respects the admissible operating conditions imposed by the H-Q predicted characteristic curves. The surrogate model of the PaT hydraulic performance is generated with *py-earth*, a library of machine-learning methods written in Python [67], and it is defined as shown in Eq. (9):

$$\begin{cases} \hat{\eta}_{PAT} = f(S, R, A, Q_{11}, n_{11}) \\ \hat{Q}_{11} = g(S, R, A, n_{11}) \end{cases} \quad (9)$$

The correlation coefficient R^2 and the generalized cross validation (GCV) [68] are used to evaluate the performance of the surrogate model.

3.6. Optimization problem

The purpose of the geometry optimization of the cutwater is to guarantee a better PAT performance in energy recovery ability, thereby reducing its energy losses. The calculations are performed in MATLAB [69] environment and the optimum geometry is detected by solving an optimization problem targeting

$$1 - \hat{\eta}_{PAT} \text{ Such that : } \begin{aligned} S &\in \Delta_S, & \hat{\eta}_{PAT} &= f(S, R, A, Q_{11}, n_{11}), \\ R &\in \Delta_R, & Q_{11} &\in \Delta_{Q11}, \\ A &\in \Delta_A, & n_{11} &\in \Delta_{N11}, \end{aligned} \quad (10)$$

The global minimum of the model function of Eq. (10) can potentially be located in the interior of the search space or on its boundaries, indicating that there might be multiple feasible regions and multiple minimum points in each region. In order to solve this non-convex problem a multi-start method is applied [70,71]: the non-linear solver runs from different starting points, reaching different locally optimal solutions. To keep high probability that the global optimal solution has been found with accuracy, a large number of runs is carried out. Therefore, approximately four thousand different initial values are used for the solver in the basin of attraction of the multi-variable global optimum value. Precisely, a systematic sampling of the search space of the independent variables S, R, A, n_{11} is set and explored in all the variable ranges.

4. Results

4.1. Validation of PaT numerical simulations

This section compares the CFD results with the available experimental data of the baseline case in order to validate the numerical model. The geometry obtained for the numerical simulation does not include the gap between the rotor and stator parts nor manufacturing tolerances. It follows that no impeller clearances have been considered. The hydraulic friction losses related and the drag loss at the back of the impeller have not been simulated, but the losses in these zones (non-flow zone losses) are mainly due to disk friction and secondary flow effects, and they can be estimated [41,72]. To reduce the discrepancy from the experimental data [47], the losses have been computed according to empirical formulations provided in literature [41,51]. The power losses created by gap friction ($\eta_f = 98\%$) and leakages ($\eta_l = 98.87\%$) have been estimated a priori, according to empirical 1-D models [51], because the pump seals and the balancing holes impeller have not simulated. In addition, the mechanical efficiency has been calculated equal to 95.4% at BEP for the size and wear of the implemented pump, also in agreement with the accepted range value 89–96% in the literature [12,51]. All these considerations allow reproducing the overall pump and PaT characteristic curves.

In Fig. 12, the PaT's specific energy coefficient, $\Psi = gH/(\omega D)^2$, and the hydraulic efficiency, η_h , of the numerical simulations are compared with the experimental data over the PaT's discharge coefficient at N_{PAT} . It should be noted that discrepancies between computations and experimental data could be partly due to the uncertainties in measurements. The uncertainty analysis gives a relative error of about $\pm 3\%$ in pressure and head at BEP operating conditions (Fig. 11).

4.2. Performance evaluation

After quality evaluations of the simulations by means of the convergence history, y_+ checks, momentum- and mass-balances, the head and efficiency outputs are analysed. In Fig. 13 – 14 – 15, the specific energy coefficient and the efficiency are shown over the

discharged unit, ϕ , normalized on the BEP of the baseline geometry and as a function of the cutwater inclination angle. All the sub-figures together give an overview of the multidimensional problem in $\phi - \Psi$ and $\phi - \eta$ for S , R , and A variables.

Interestingly, stretching the cutwater produces a considerable increase of the PaT required available head, and shifts the efficiency peaks at lower discharges: by extending the cutwater length from two to four times, Ψ increases on average by 25% and 32% at low and high discharge, respectively. In this way, the flow leans along the cutwater walls favouring a tangential component at the entrance of the runner. Due to the absence of diffuser vanes, the

first approximation of α_2 is given by the cutwater incidence [51]. Therefore, in turbine operation, the volute determines the runner absolute flow angle, α_2 , which directly affects the theoretical specific energy of the turbine, as expressed in Eq. (2).

Moreover, the cutwater tip, R , slightly influences the specific energy coefficient, Ψ , except if the cutwater is characterized by a large stretching ($S > 3L$) and at high negative tilt angle ($A = -25^\circ$). In these conditions, the head output is inversely proportional to the thickness of the cutwater tip: a sharp rounding $R = r/4$ produces an 18–20% raise in head compared to the baseline rounding ($R = r$).

Furthermore, it is highlighted that an excess of negative

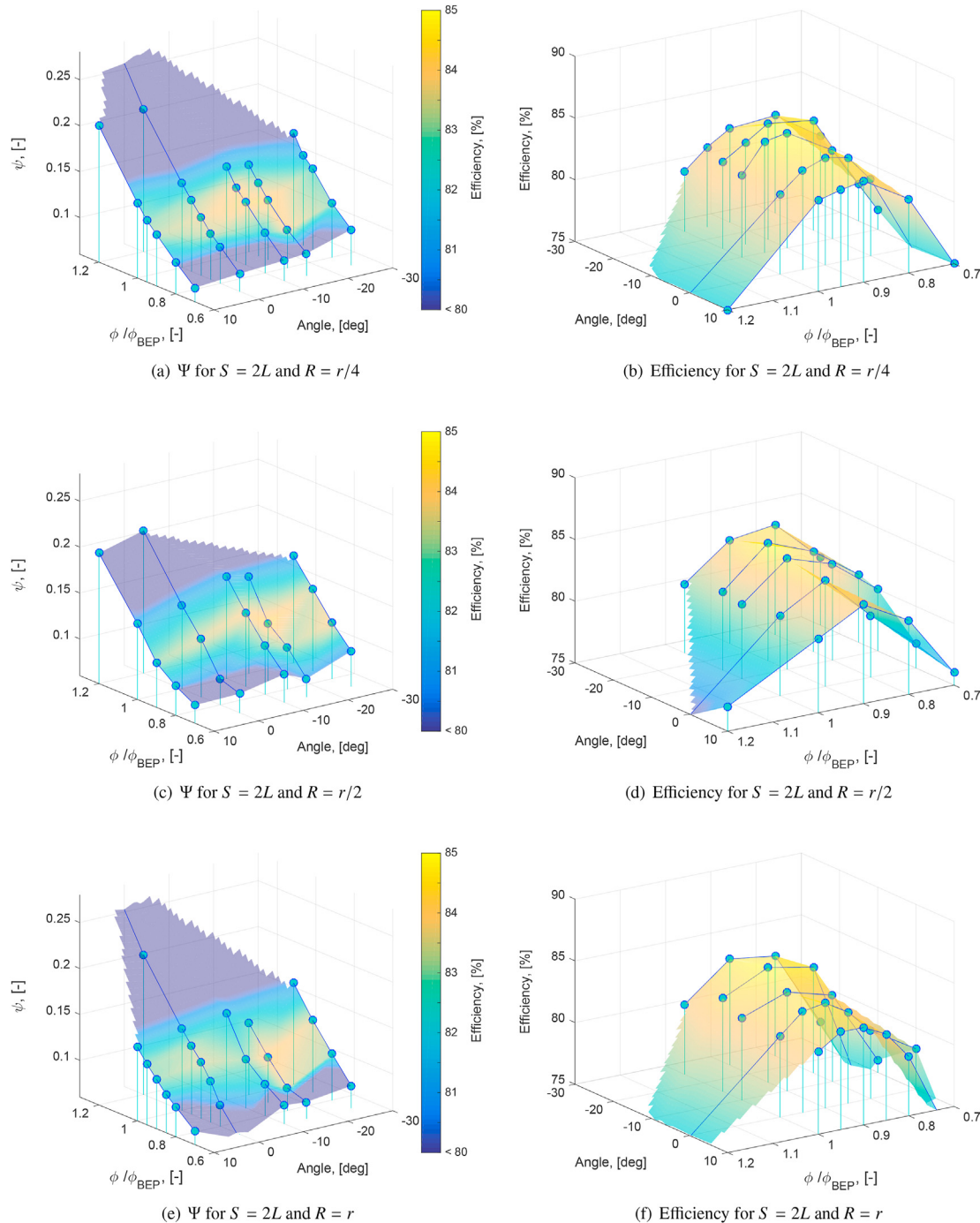


Fig. 13. Head characteristics as a function of the discharge number and the cutwater angle for $S = 2L$.

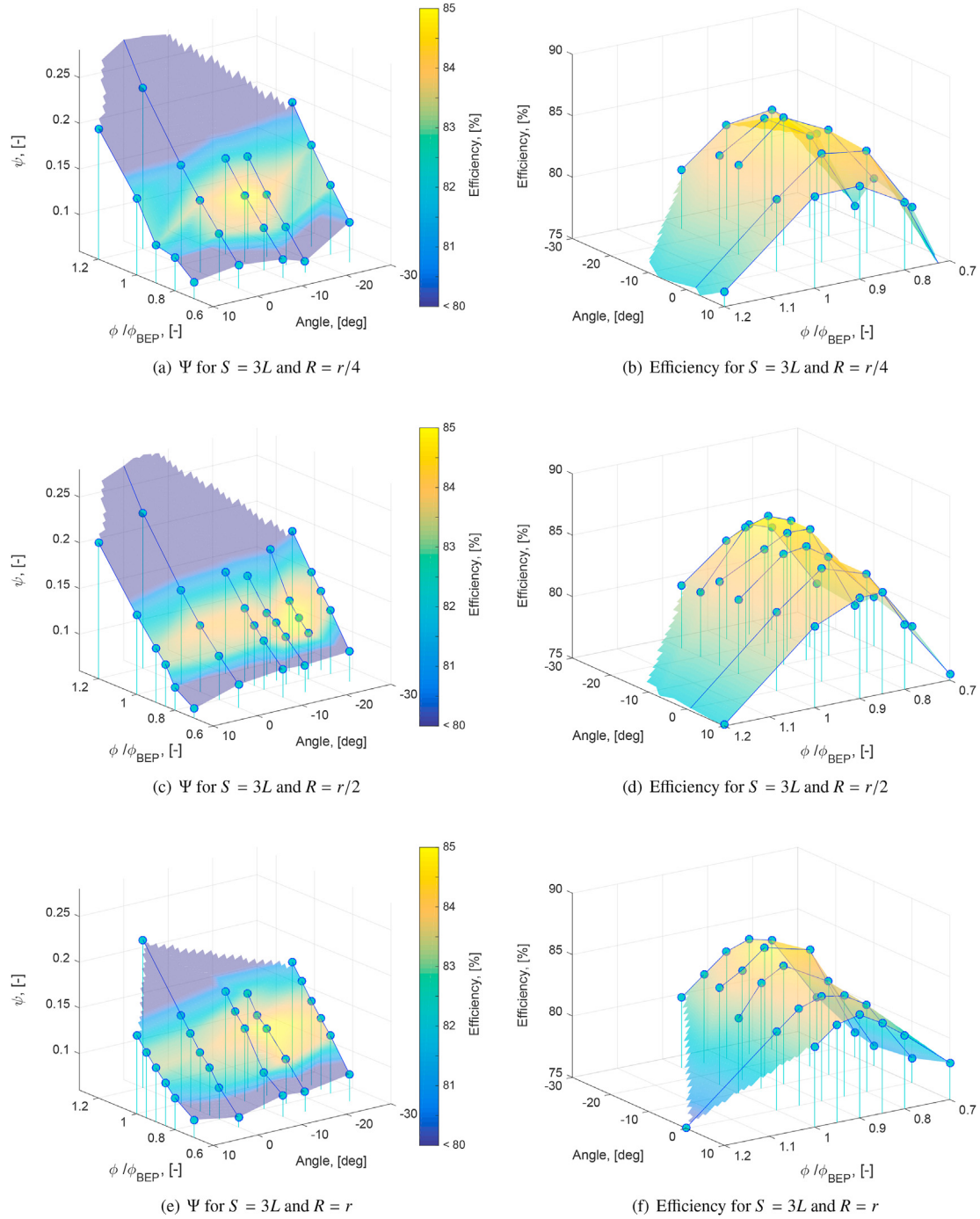


Fig. 14. Head characteristics as a function of the discharge number and the cutwater angle for $S = 3L$.

inclination, A , causes an increase of the specific energy coefficient Ψ , between +0.04 and + 0.08 in respect to the baseline characteristics. The water streamlines are stirred towards the outer wall of the volute, by rising considerably the absolute velocity circumferential component c_{2u} but also turbulence. As a consequence, the efficiency drops at high negative inclination. Positive inclination ($A = + 10^\circ$) globally reduces both specific energy and hydraulic efficiency.

To provide a quantification of the numerical accuracy, the numerical standard deviation of the mass flow balance are given. In Fig. 16, the errors computed during the CFD simulations over the discharge unit, ϕ , are normalized on the BEP of the baseline

geometry. From the performance evaluation, it emerges that a longer cutwater pushes the peak of efficiency at lower discharge. As a result, numerous tests occur in $0.7 < \phi/\phi_{BEP} < 0.9$, where most of the new design BEPs lay and the mass-error drops below 1%.

4.3. Surrogate model of the PaT hydraulic performance

The surrogate model of $\hat{\eta}_{PAT}$ is built according the formulations expressed in Eq. (9). The complementary definition of \hat{Q}_{11} links $\hat{\eta}_{PAT}$ to the constraints of the PaT hydraulic characteristics. The training data-set to build each surrogate model is obtained by randomly selecting 80% of the 224 simulated operating conditions

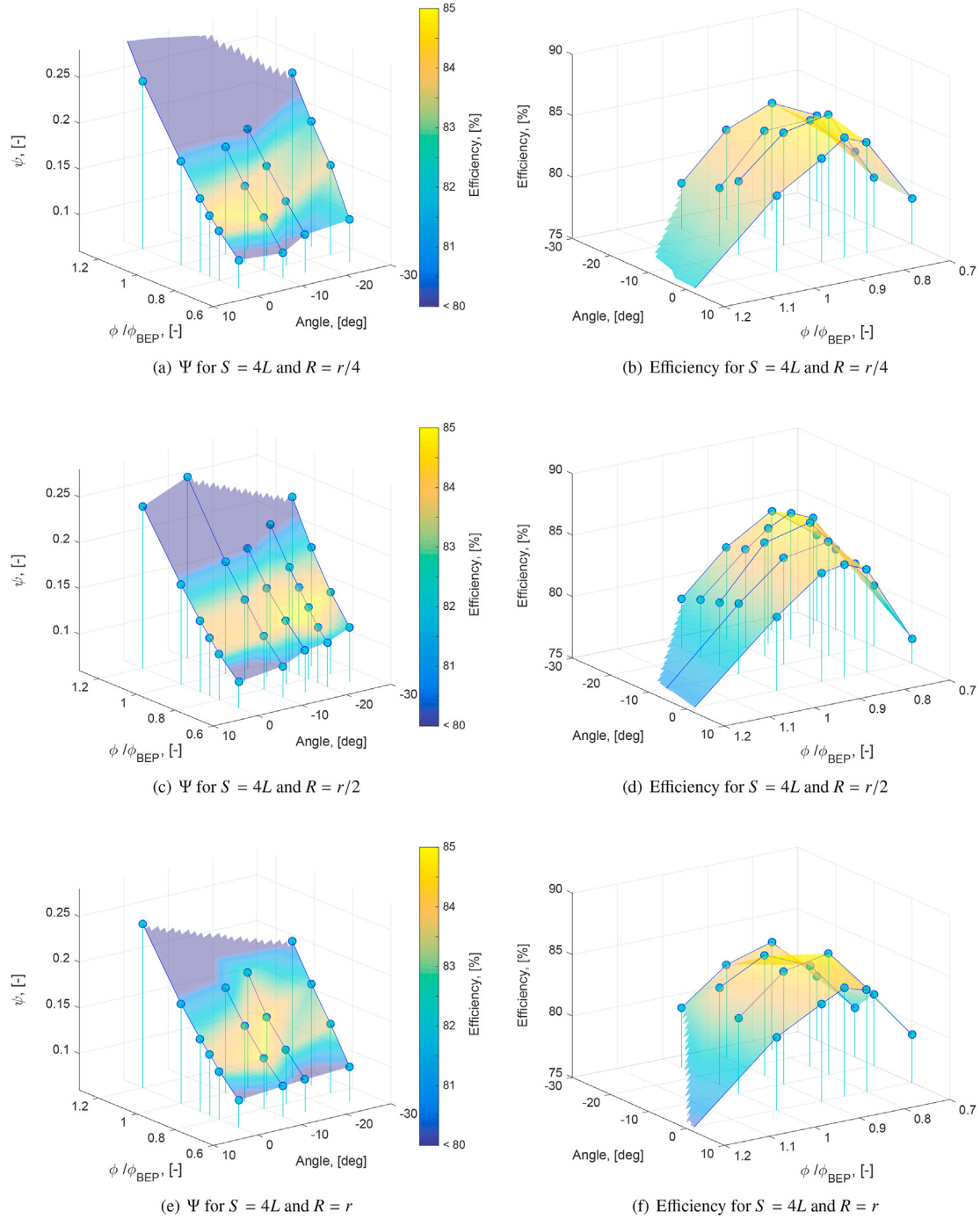


Fig. 15. Head characteristics and efficiency as a function of the discharge number and the cutwater angle for $S = 4L$.

and the test data-set is composed by the earmarked 20% of the samples. The surrogate model $\hat{\eta}_{PAT}$ as a function of the cutwater dimensions and operating points is calculated and detailed in the Appendix (Table 6). Similarly, the formulation for \hat{Q}_{11} consists of only 16 enabled terms which are listed in the Appendix (Table 7). A quadratic degree of the fitting terms for $\hat{\eta}_{PAT} = g(S, R, A, Q_{11}, n_{11})$ is found satisfactory and it includes a cubic expression of \hat{Q}_{11} equally reliable. Fig. 17 illustrates the histogram of the model prediction error on the test data-set, and it assures the limited misstep of the surrogate model: 90% of the tested data records an error within \pm

1%. Likewise, another test on the Q_{11} function is performed and its results confirm the good accuracy of the model (Fig. 18). The resulting values of R-squared and GCV are found to be adequate both for the \hat{Q}_{11} constrain function (R-squared = 0.98 and GCV = 0.0002) and for the $\hat{\eta}_{PAT}$ final formulation (R-squared = 0.96 and GCV = 0.9906).

4.4. Optimal cutwater design

For each feasible n_{11} , a global optimal solution is retrieved by

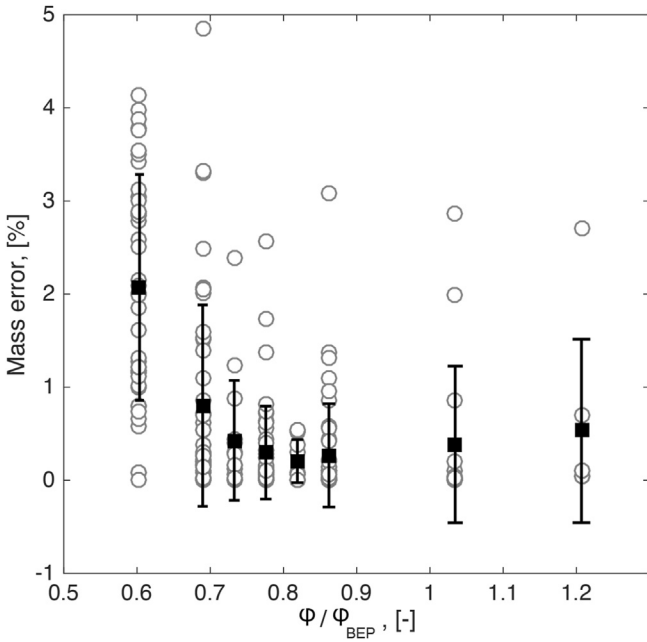


Fig. 16. Numerical error for mass-flow mismatch between the inlet and outlet over the relative discharge number ϕ/ϕ_{BEP} for 224 simulations.

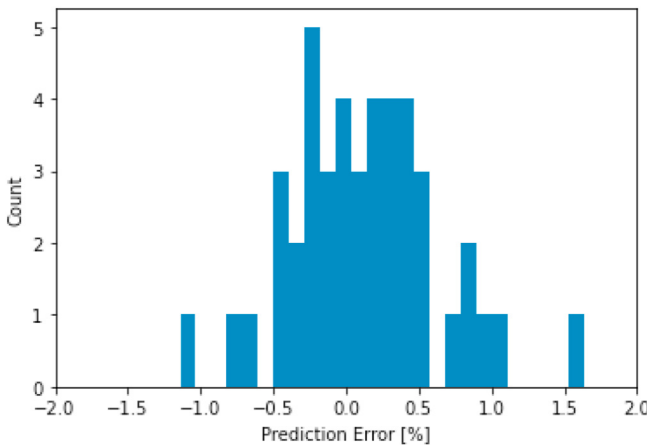


Fig. 17. Test model accuracy for $\hat{\eta}_{PAT} = f(S, R, A, Q_{11}, n_{11})$.

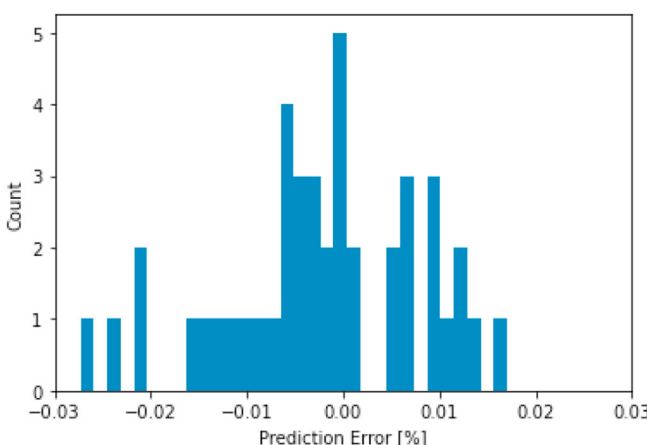


Fig. 18. Test model accuracy for $\hat{Q}_{11} = g(S, R, A, n_{11})$.

solving Eq. (10). In **Table 5**, the efficiency values of the optimal geometry conditions found by solving the optimization problem are highlighted for different n_{11} values. The predicted peak of efficiency is found at $n_{11} = 84.303$, corresponding to the set of variables: $S_{opt} = 3.54L$, $R_{opt} = r$ and $A_{opt} = -15^\circ$. The resulting optimized geometry has been simulated and the relative errors in Eq. (10) show the modest discrepancy between the prediction and the simulations outputs of the optimal cutwater design:

$$\begin{aligned}\Delta\phi &= \frac{\hat{\phi} - \phi_{opt}}{\phi_{opt}} = 0.01877 \\ \Delta\Psi &= \frac{\hat{\Psi} - \Psi_{opt}}{\Psi_{opt}} = -0.07833 \\ \Delta\eta &= \frac{\hat{\eta} - \eta_{opt}}{\eta_{opt}} = -0.00478\end{aligned}\quad (11)$$

Fig. 19 compares the PaT characteristics curves with the baseline cutwater and the optimized geometry. Although the BEP moves to 13.0% smaller discharge, the updated PaT cutwater records a raise in head by +7.5% and the final gain in hydraulic efficiency is $\eta_{opt} - \eta = +3.9$. Therefore, significant improvements of the efficiency are reported at lower discharge in the broad range of $\phi/\phi_{BEP} = 0.6 - 0.9$, while the geometry update equalizes the baseline design for larger discharge values ($\phi/\phi_{BEP} > 1$).

In common hydraulic turbines, guide vanes are used to regulate the discharge and to impart a degree of swirl to the flow determined by the needs of the runner. Similarly, the water flow from the PaT inlet could be deflected by the cutwater towards tangential direction and improve the efficiency. In the PaT baseline design, this deviation is not sufficient and an unbalanced water distribution occurs near the rotor/stator gap. In this way, a pump in reverse mode experiences a non-uniform speed and pressure profiles along the leading edge of the runner, generating local flaws in the velocity field in the cutwater area. In **Fig. 20**, the static pressure profile along the arc length mid-flow of the half rotor/stator interface in front of the cutwater (location marked with a dashed line) is illustrated for the baseline geometry and the optimized design. In the contour plots, the pressure coefficient C_p , defined as in Eq. (12), shows the effect of the new cutwater length and angle in dissipating this pressure peak on the rotor/stator interface by transferring radial flow into circumferential flow:

$$C_p = 2 \frac{P - P_{inlet}}{\rho V_{inlet}^2} \quad (12)$$

To validate the new incidence distribution at the runner inlet generated by the new design, the absolute velocity angle is compared to the volute mid-flow plan across the volute (**Fig. 21**). A shorter cutwater corresponds to smaller flow deviation, allowing for a higher value of radial velocity in the near-cutwater region and

Table 5
Predicted optimal cutwater geometry and resulting efficiency by varying n_{11} .

$n_{11} [-]$	$S [mm]$	$R [mm]$	$A [deg]$	$\hat{Q}_{11} [-]$	$\hat{\eta} [\%]$
110.378	60.40	65.0	-18.36	0.4364	79.00
103.250	56.67	65.0	-15.60	0.4107	80.91
97.345	56.25	65.0	-14.93	0.4107	83.33
92.349	55.94	65.0	-14.81	0.4106	84.68
88.051	55.63	65.0	-14.80	0.4106	85.32
84.303	55.11	65.0	-15.14	0.4106	85.48
80.996	24.21	60.0	-24.22	0.3435	84.12

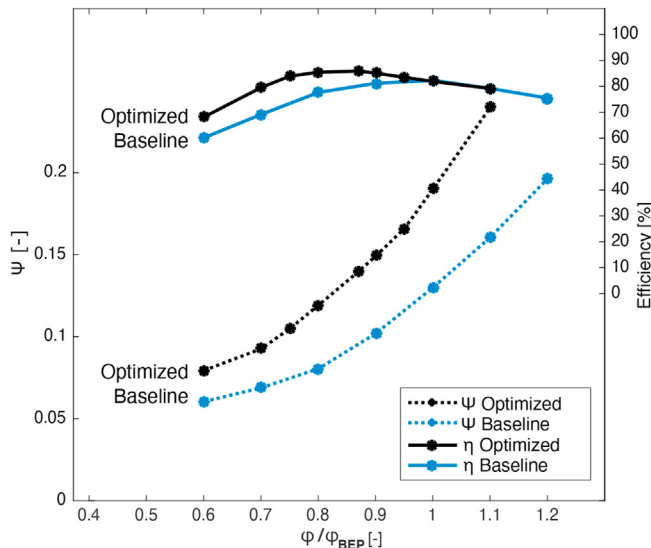


Fig. 19. Ψ and η characteristics of the baseline and optimal cutwater design at N_{PAT} .

higher turbulence on the runner inlet. Over an arc of 28° , the absolute velocity angle α_2 overpasses 0.75 rad at the mid-span flow before the runner inlet, raising the averaged value at the R/S interface to 0.48 rad in the baseline design. In the optimized design, the averaged value of α_2 is 0.28 rad.

concerning the distribution of turbulent kinetic energy, k , the region with a high intensity involves the core flow in the volute for the baseline design and the volute outer wall surface of volute for

the optimized design Fig. 22. For both cases, the highest gradients of k in the flow field are concentrated downstream the cutwater. Here, a peak of water turbulent kinetic energy occurs and indicates that the flow is relatively complex and with stronger velocity fluctuations. However, in the optimized solution the cutwater improves the turbulence kinetic energy distribution stability in the mid-flow, where k is reduced to near zero, and clearing the passage towards the runner inlet.

4.5. Development of speed adjustment

The cutwater design generated by the solution of the optimization problem has improved the hydraulic efficiency and altered the PaT performance characteristics from its initial condition (Fig. 19). The definition of the optimized BEP operating condition, to meet the original required head at $\phi/\phi_{BEP} = 1$, is achieved by operating at a different rotational speed. Rotational speed adjustments are commonly used to deal with variable load: varying the shaft speed allows modifying the relative flow angles which provides higher performance [73,74]. To respect the similarity laws, the non-dimensional parameters obtained at different speeds shall collapse on a quadratic line [38]. It appears that Ψ and η curves distinctly converge for both optimized and baseline cases, as represented in Fig. 23. The PaT with the original geometry has been simulated for $\Omega = [0.85, 1.28]$ and the optimized geometry within $\Omega = [0.85, 1.14]$, where Ω is the rotational speed ratio N/N_{PAT} . A quadratic polynomial fits the data for the specific energy coefficient by the least squares method (R-squared equals 0.9733), whereas a cubic regression returns the best fit for η but it does not entirely interpret the data-set (R-squared equals 0.8365). Besides inevitable numerical errors of the model and the geometrical assumptions,

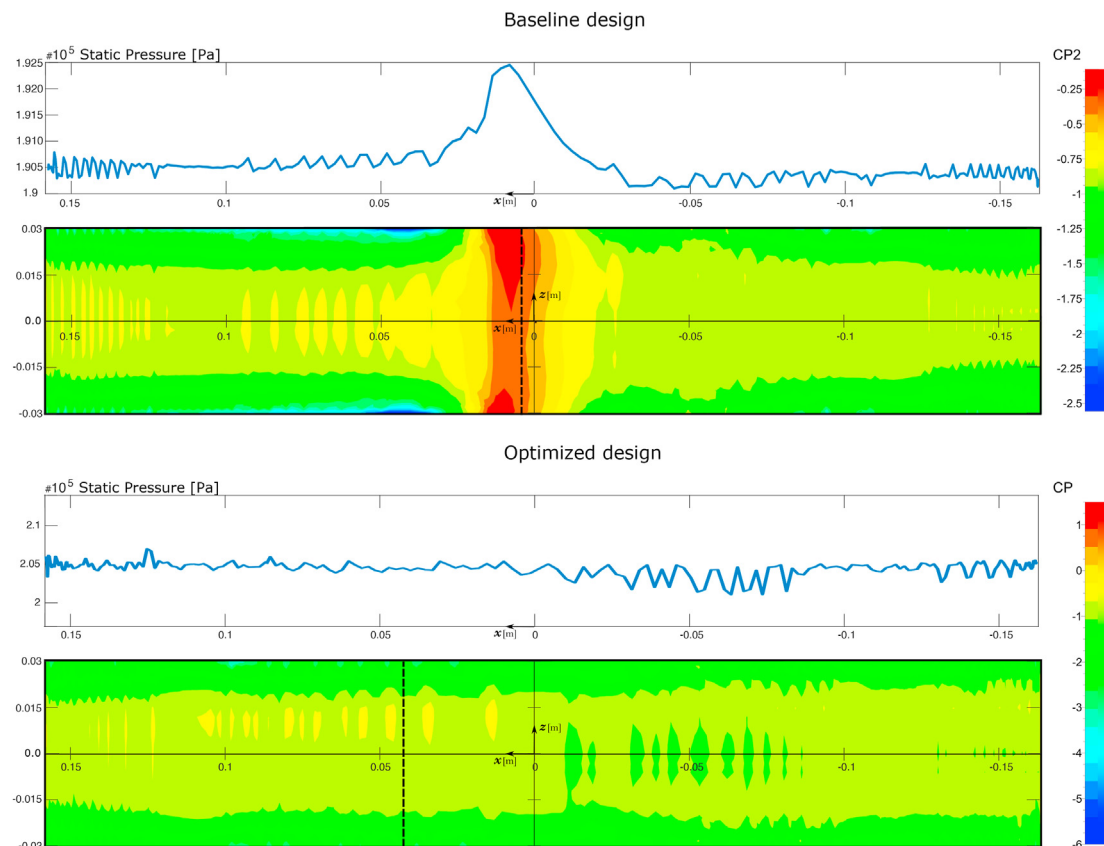


Fig. 20. Static pressure profiles at mid-span and C_p contour for the rotor/stator interfaces in both baseline and optimized cutwater geometry.

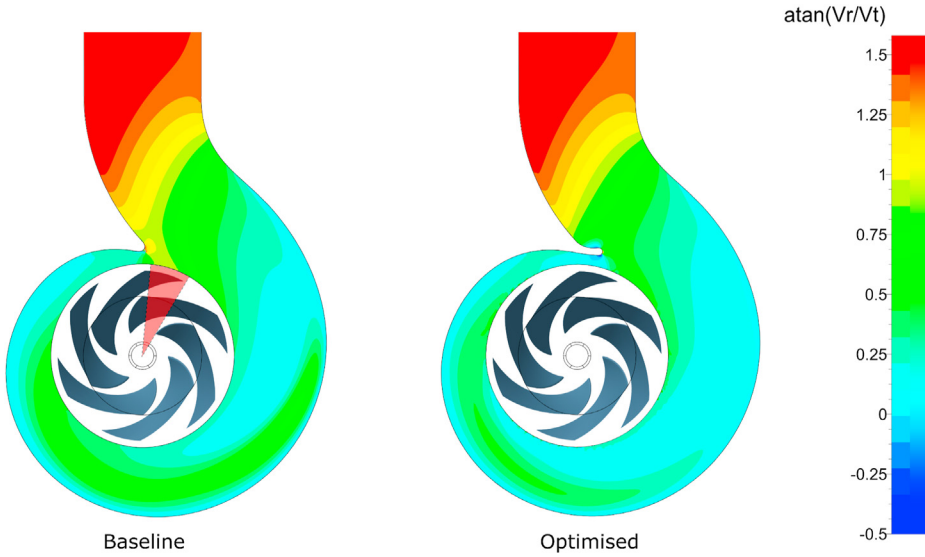


Fig. 21. Contours of the absolute velocity angle α_2 [rad] across the volute cut-view. In the baseline design, the arc of high α_2 is pointed out.

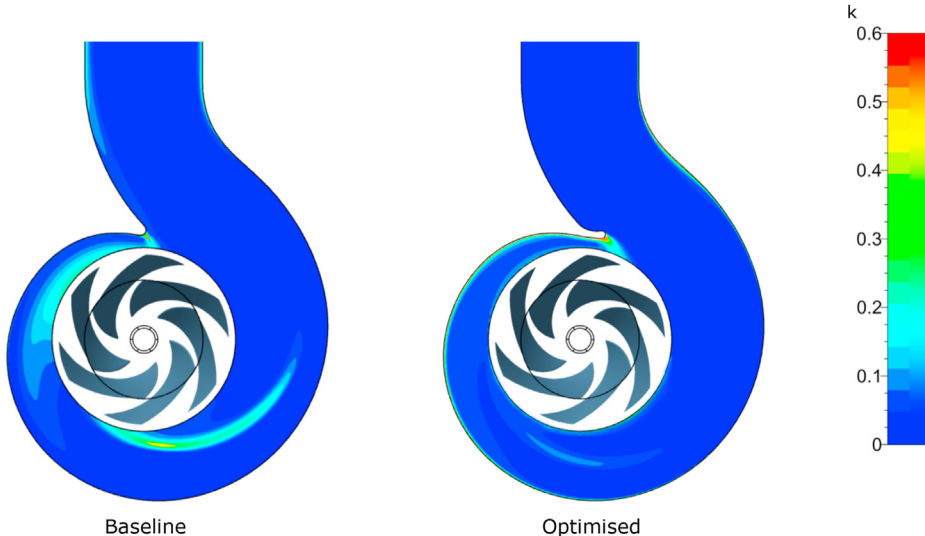


Fig. 22. Contours of the turbulence kinetic energy k [m^2/s^2] distribution across the volute cut-view.

these deviations are also due to the different losses distribution for different rotational speeds. The similarity laws are basically an approximation, based on the assumption of geometrical and dynamic similarity between the pump working under different conditions, but certain considerations must be taken into account [38,75]. At high discharge, the friction losses are more accentuated in a convergent channel (as in a pump in reverse mode) and they mark the upper hydrodynamic limit on the maximum rotational speed [76]. On the other hand, low discharge generates substantial shock losses in PaTs [77], thus low rotational speed are not recommended.

Fig. 24 shows an enlarged detail of Fig. 23 and it illustrates the effect of the speed variation ($\pm 14\%$) on the PaT efficiency. The following regression equation describes the PaT hydraulic efficiency depending on ϕ and Ω :

$$\eta_{BEP} = a_1\phi + a_2 + a_3\Omega \quad (13)$$

with the coefficients equal to $a_1 = 79.45$, $a_2 = 80.54$ and $a_3 =$

4.22, $R^2 = 0.959$ is obtained. According to the analysis of the PaTs performance at different rotational speeds, corrections on the similarity law can be made in $a\left(\frac{N}{N_{ref}}\right)^b$ form by Eq.(14). A new formulation can be applied to predict the hydraulic efficiency by Eq.(15).

$$Q / Q_{ref} = 0.984 \Omega^{0.958} \quad H / H_{ref} = 0.970 \Omega^{1.920} \quad (14)$$

$$\eta / \eta_{ref} = -0.047 \Omega^2 + 0.1521 \Omega + 0.8951 \quad (15)$$

According to these correlations, a rotational speed adjustment by 2% (i.e. -15 rpm) allows reducing the available head from the H_{opt} to the initial baseline value, as such $H / H_{ref} = 1 / 1.075$, with a negligible effect on the efficiency ($\eta / \eta_{ref} = 0.9989$).

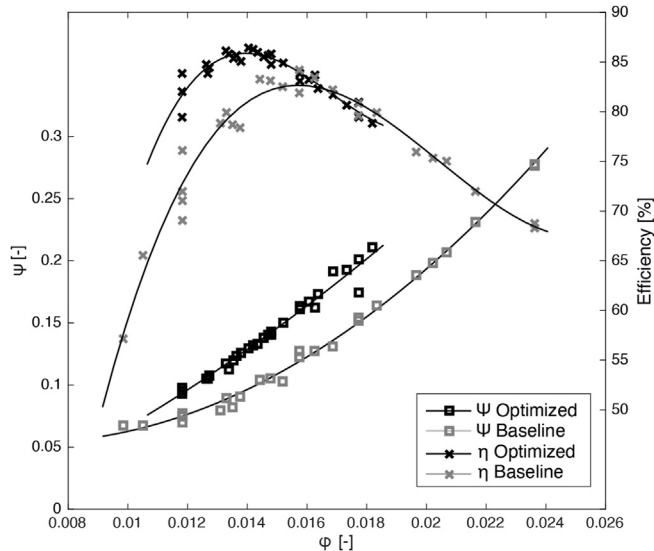


Fig. 23. PaT performances with the baseline and optimal cutwater designs for $\Omega = [0.85, 1.28]$.

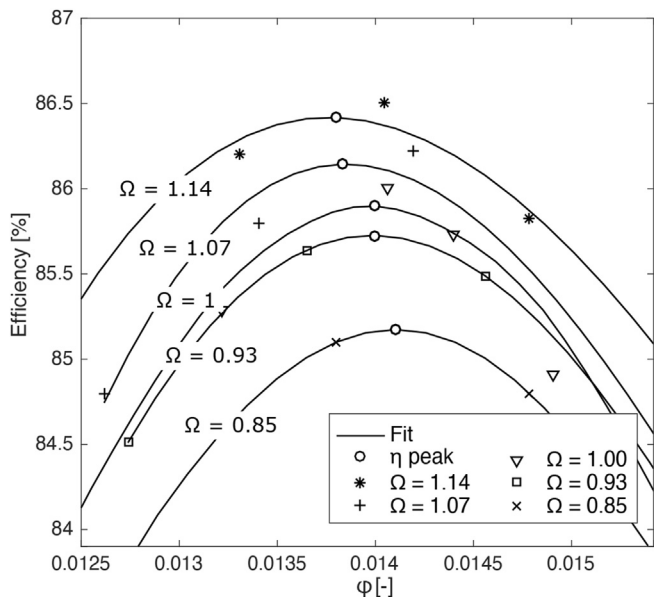


Fig. 24. Detail of the PaT efficiency in Fig. 23 for the optimized geometry under speed variations Ω .

5. Conclusions

In this work, a novel cutwater design is provided for improving the hydraulic efficiency of a PaT. A numerical investigation is computed for 224 operating conditions to establish a surrogate model of the PaT performance according to its cutwater geometry and characteristics. Firstly, the research addresses the modification of the cutwater geometry in terms of length, rounding (or tip thickness) and angle (or tilt deviation). Then, the numerical simulations of the PaT baseline considering the initial cutwater design are validated by the experimental data available from the micro PHES system where this centrifugal pump is installed [62]. The specific energy coefficient and efficiency characteristic curves are obtained for the modified cutwater. The results highlight the influence of the cutwater geometry in deflecting the inlet flow in the

runner for improved performance. With a longer cutwater and within a limited range of the inclinations, the PaT's BEP moves to higher head but lower discharge and a considerable improvement in efficiency is obtained. Additional numerical simulations under unsteady state with a 360° impeller have been performed in [78] to validate the optimum obtained with the methodology presented in this article. Further investigations would require to deeply investigate the transient phenomena driven by the cutwater modifications such as dynamic pulsations, vortex formation and cavitation. However, the CFD results here computed are already in good agreement with the measurements within the accuracy of the experiments and the assumption of steady flow. Moreover, this configuration allows preserving the celerity of the methodology proposed, because an unsteady simulation, that requires a mesh with multiple blade passage and an adequate number of time-step, would need a computational effort about ten times greater than a steady state simulation.

Thanks to the outcomes achieved by the numerical simulations, a sufficient data-set of the PaT performance is available to train, validate and test a multivariate regression method. This process builds a model of the PaT efficiency as a function of the operating conditions and the cutwater geometrical parameters. By solving the optimization problem targeting the maximization of the PaT efficiency, the best cutwater geometry is found. This allows a drastic shortening of the investigation time. Solving the complete optimization problem lasts less than one-tenth of the execution time needed for a single set point CFD simulation.

The model results converged on a new cutwater design and the PaT BEP gains 3.9% in hydraulic efficiency, which is an outstanding performance improvement that doesn't require to modify the pump impeller. The new BEP operates close to the nominal operating conditions of the baseline cutwater geometry at 87% of the discharge and for 107.5% of the available head. The change in operating condition reduces the theoretical power generation of the micro-turbine. However, such power subtraction is almost fully compensated by the performance improvement of the cutwater modification. Moreover, because the water volume of the upper reservoir is unaffected, the energy capacity of the hydropower system of the investigated PaT is augmented accordingly to its efficiency. In this way, the micro hydropower facility generates approximately the same power output and the water resource is exploited more responsibly. Variable speed technology is also foreseen and studied in order to revise the operating condition: a modest –2% correction of the rotational speed allows the available head of the optimized PaT to be adjusted according the initial baseline requirement.

The outcomes of this study deliver a methodology which can be employed for a systematic volute adjustment by reducing the computational time and to promote furthermore the employment of PaTs in micro/minihydropower applications.

CRediT authorship contribution statement

Alessandro Morabito: Conceptualization, Methodology, Software, Investigation, Writing – original draft. **Elena Vagnoni:** Methodology, Writing – review & editing. **Mariano Di Matteo:** Formal analysis. **Patrick Hendrick:** Supervision, Funding acquisition.

Declaration of competing interest

The authors declare that they have no known competing financial interests or personal relationships that could have appeared to influence the work reported in this paper.

Acknowledgements

This research has been supported by SmartWater project (Service Public Wallonie SPW-DGO4) and FlexWatter project (Service public fédéral Économie - Energy Transition Fund of Belgium).

Appendix. tables

Table 6

Basis functions for $\hat{\eta}_{PAT}$ by the variables S, R, A Q_{11} , and n_{11} .

Basis Function	Pruned	Coefficient
(Intercept)	No	84.2996
$h(n_{11} - 81.3415)$	Yes	None
$h(81.3415 - n_{11})$	No	0.917686
$Q_{11} * h(81.3415 - n_{11})$	No	-3.0256
$h(Q_{11} - 0.451706) * h(n_{11} - 81.3415)$	No	8.12082
$h(0.451706 - Q_{11}) * h(n_{11} - 81.3415)$	No	-4.7669
$h(n_{11} - 84.1156) * h(n_{11} - 81.3415)$	No	-0.0134891
$h(84.1156 - n_{11}) * h(n_{11} - 81.3415)$	Yes	None
$n_{11} * h(81.3415 - n_{11})$	Yes	None
$S * h(n_{11} - 81.3415)$	No	0.00384514
$h(Q_{11} - 0.408705)$	Yes	None
$h(0.408705 - Q_{11})$	Yes	None
$A * h(n_{11} - 81.3415)$	No	-0.00216247
$h(Q_{11} - 0.412572) * h(Q_{11} - 0.408705)$	Yes	None
$h(0.412572 - Q_{11}) * h(Q_{11} - 0.408705)$	No	290637
$A * h(Q_{11} - 0.408705)$	No	-1.27544
$S * h(Q_{11} - 0.408705)$	Yes	None
$n_{11} * h(Q_{11} - 0.408705)$	No	-0.439592
$h(n_{11} - 75.4268) * h(81.3415 - n_{11})$	Yes	None
$h(75.4268 - n_{11}) * h(81.3415 - n_{11})$	No	-0.0109386
$A * h(0.408705 - Q_{11})$	Yes	None

Table 7

Basis functions for \hat{Q}_{11} by the variables S, R, A, and n_{11} for third degree maximum fit spline.

Basis Function	Pruned	Coefficient
(Intercept)	No	0.497193
A	No	0.000802073
S	No	-0.00603202
R	Yes	None
$h(n_{11} - 106.309) * S$	No	0.000183678
$h(106.309 - n_{11}) * S$	Yes	None
$A * h(106.309 - n_{11}) * S$	No	5.99249e-06
A^2	No	0.00014047
A^3	No	5.7401e-06
$R * A$	Yes	None
$h(n_{11} - 102.63)$	No	-0.00411946
$h(102.63 - n_{11})$	Yes	None
$n_{11} * R$	Yes	None
$h(n_{11} - 96.0777) * h(102.63 - n_{11})$	Yes	None
$h(96.0777 - n_{11}) * h(102.63 - n_{11})$	Yes	None
$S * n_{11} * R$	No	-1.3619e-07
$A * h(102.63 - n_{11})$	No	-5.27589e-05
$S * R * A$	No	-6.76829e-07
$R * A^2$	No	-8.57713e-07
$S * A * h(102.63 - n_{11})$	No	-4.80337e-06
$A * h(n_{11} - 96.0777) * h(102.63 - n_{11})$	Yes	None
$R^2 * n_{11}$	No	9.76616e-08
$R * S$	Yes	None
$S^2 R$	Yes	None
S^2	No	0.000152352
S^3	No	-1.27029e-06

Nomenclature

<i>B</i>	Systematic error	-
<i>c</i>	Absolute velocity	m/s
<i>Cp</i>	Static pressure coefficient	-
<i>D</i>	Diameter	m
<i>E</i>	Specific energy	J/kg
<i>h</i>	Hinge function factor	-
<i>H</i>	Head	m
<i>k</i>	Turbulent kinetic energy	m/s
<i>L</i>	Nominal cutwater length	mm
<i>M</i>	Torque	Nm
<i>n</i> ₁₁	Unit speed	-
<i>n_d</i>	Number of mesh nodes	-
<i>N</i>	Rotational speed	rpm
<i>N_s</i>	Specific speed	m, m/s
<i>Q</i>	discharge	m/s
<i>Q</i> ₁₁	Unit discharge	-
<i>r</i>	Nominal cutwater radius	mm
<i>u</i>	Peripheral velocity	m/s
<i>V</i>	Volume	m
<i>w</i>	Relative velocity	m/s
α	Absolute velocity angle	rad
β	Relative velocity angle	rad
η	Efficiency	-
λ	Blade inclination	rad
φ	Discharge number	-
ω	Angular speed	rad/s
Ω	Speed ratio	-
Ψ	Specific energy coefficient	-

Subscripts	
1	PaT outlet
2	PaT inlet
<i>h</i>	Hydraulic
<i>l</i>	Loss
<i>m</i>	Meridional
<i>opt</i>	Optimal
<i>vol</i>	Volumetric

References

- [1] D. Connolly, H. Lund, B.V. Mathiesen, Smart Energy Europe: the technical and economic impact of one potential 100% renewable energy scenario for the European Union, Renew. Sustain. Energy Rev. (2016).
- [2] IEA, Renewables information 2019 overview, Climate Change 2013 - The Physical Science Basis 53 (9) (2019) 1–30.
- [3] A.A. Khan, A.M. Khan, M. Zahid, R. Rizwan, Flow acceleration by converging nozzles for power generation in existing canal system, Renew. Energy 60 (2013) 548–552.
- [4] O. Tamm, T. Tamm, Verification of a robust method for sizing and siting the small hydropower run-of-river plant potential by using GIS, Renew. Energy 155 (2020) 153–159.
- [5] G.C. de Andrade Furtado, A.L. Amarante Mesquita, A. Morabito, P. Hendrick, J.D. Hunt, Using hydropower waterway locks for energy storage and renewable energies integration, Appl. Energy 275 (2020) 115361.
- [6] M. Crespo Chacón, J.A. Rodríguez Díaz, J. García Morillo, A. McNabola, Estimating regional potential for micro-hydropower energy recovery in irrigation networks on a large geographical scale, Renew. Energy 155 (2020) 396–406.
- [7] Z.-k. Feng, W.-j. Niu, C.-t. Cheng, “China’s large-scale hydropower system: operation characteristics, modeling challenge and dimensionality reduction possibilities, Renew. Energy 136 (2019) 805–818.
- [8] A.A. Khan, A. Shahzad, I. Hayat, M.S. Miah, Recovery of flow conditions for optimum electricity generation through micro hydro turbines, Renew. Energy 96 (2016) 940–948.
- [9] A. Carravetta, O. Fecarotta, M. Sinagra, T. Tucciarelli, Cost-benefit analysis for hydropower production in water distribution networks by a pump as turbine, J. Water Resour. Plann. Manag. (2014).
- [10] S.V. Jain, R.N. Patel, Investigations on pump running in turbine mode: a review of the state-of-the-art, Renew. Sustain. Energy Rev. 30 (2014) 841–868.
- [11] M. Binama, W.T. Su, X.B. Li, F.C. Li, X.Z. Wei, S. An, Investigation on pump as turbine (PAT) technical aspects for micro hydropower schemes: a state-of-the-art review, Renew. Sustain. Energy Rev. 79 (2017) 148–179.
- [12] D.R. Giosio, A.D. Henderson, J.M. Walker, P.A. Brandner, J.E. Sargison, P. Gautam, Design and performance evaluation of a pump-as-turbine micro-hydro test facility with incorporated inlet flow control, Renew. Energy 78 (2015) 1–6.
- [13] S. Baumgarten, W. Guder, Pumpen Als Turbinen vol. 11, KSB Pump company,

- 2005, pp. 2–9. Technik kompakt.
- [14] K.H. Motwani, S.V. Jain, R.N. Patel, Cost analysis of pump as turbine for pico hydropower plants - a case Study, Procedia Engineering (2013).
- [15] M. Arriaga, Pump as turbine - a pico-hydro alternative in Lao People's Democratic Republic, Renew. Energy (2010).
- [16] H. Ramos, A. Borga, Pumps as turbines: an unconventional solution to energy production, Urban Water (1999).
- [17] B. Teuteberg, Design of a pump-as-turbine microhydro system for an abalone farm, M.Engineering (2010).
- [18] F. Pugliese, F. De Paola, N. Fontana, M. Giugni, G. Marini, Experimental characterization of two Pumps as Turbines for hydropower generation, Renew. Energy (2016).
- [19] A.A. Williams, The Turbine Performance of Centrifugal Pumps: A Comparison of Prediction Methods, 1994.
- [20] A.J. Stepanoff, Centrifugal and Axial Flow Pumps: Theory, Design, and Application, Wiley, New York, 1957.
- [21] E. Schmiedl, Serien-kreiselpumpen im turbinenbetrieb, *Pumpentagung: Karlsruhe*, Germany, 1988.
- [22] H. Nautiyal, A. Kumar, S. Yadav, Experimental investigation of centrifugal pump working as turbine for small hydropower systems, Energy Sci. Technol. 1 (1) (2011) 79–86, <https://doi.org/10.3968/j.est.1923847920110101.006>.
- [23] M. Rossi, M. Renzi, Analytical prediction models for evaluating pumps-as-turbines (PATs) performance, Energy Procedia (2017).
- [24] S.S. Yang, S. Derakhshan, F.Y. Kong, Theoretical, numerical and experimental prediction of pump as turbine performance, Renew. Energy 48 (2012) 507–513, <https://doi.org/10.1016/j.renene.2012.06.002>.
- [25] S. Barbarelli, M. Amelio, G. Florio, Predictive model estimating the performances of centrifugal pumps used as turbines, Energy (2016).
- [26] A. Caravetta, G. Del Giudice, O. Fecarotta, H.M. Ramos, Pump as turbine (PAT) design in water distribution network by system effectiveness, Water (Switzerland) (2013).
- [27] A. Caravetta, O. Fecarotta, H.M. Ramos, A new low-cost installation scheme of PATs for pico-hydropower to recover energy in residential areas, Renew. Energy (2018).
- [28] Z. Qian, F. Wang, Z. Guo, J. Lu, Performance evaluation of an axial-flow pump with adjustable guide vanes in turbine mode, Renew. Energy (2016).
- [29] A. Morabito, J. Steimes, O. Bontems, G. Al Zohbi, P. Hendrick, Set-up of a pump as turbine use in micro-pumped hydro energy storage: a case of study in Froyennes Belgium, in: Journal of Physics: Conference Series, 2017.
- [30] S.C. Miao, J.H. Yang, G.T. Shi, T.T. Wang, Blade profile optimization of pump as turbine, Adv. Mech. Eng. (2015).
- [31] S. Derakhshan, B. Mohammadi, A. Nourbakhsh, Efficiency improvement of centrifugal reverse pumps, J. Fluid Eng. (2009). Transactions of the ASME.
- [32] S.N. Asomani, J. Yuan, L. Wang, D. Appiah, K.A. Adu-Poku, The impact of surrogate models on the multi-objective optimization of Pump-As-Turbine (PAT), Energies (2020).
- [33] T. Wang, C. Wang, F. Kong, Q. Gou, S. Yang, Theoretical, experimental, and numerical study of special impeller used in turbine mode of centrifugal pump as turbine, Energy (2017).
- [34] M.B. Patel, R.N. Mevada, D. Sardana, V.P. Rajput, Experimental and numerical investigation of centrifugal pump performance in reverse mode, Int. J. Adv. Technol. Eng. Sci. (2015).
- [35] S.S. Yang, C. Wang, K. Chen, X. Yuan, Research on blade thickness influencing pump as turbine, Adv. Mech. Eng. (2014).
- [36] S.S. Yang, F.Y. Kong, W.M. Jiang, X.Y. Qu, Effects of impeller trimming influencing pump as turbine, Computers and Fluids (2012).
- [37] S.S. Yang, H.L. Liu, F.Y. Kong, C. Dai, L. Dong, Experimental, numerical, and theoretical research on impeller diameter influencing centrifugal pump-as-turbine, J. Energy Eng. (2013).
- [38] S.V. Jain, A. Swarnkar, K.H. Motwani, R.N. Patel, Effects of impeller diameter and rotational speed on performance of pump running in turbine mode, Energy Convers. Manag. (2015).
- [39] S.S. Yang, F.Y. Kong, H. Chen, X.H. Su, Effects of blade wrap angle influencing a pump as turbine, J. Fluid Eng. (2012). Transactions of the ASME.
- [40] P. Singh, F. Nestmann, Internal hydraulic analysis of impeller rounding in centrifugal pumps as turbines, Exp. Therm. Fluid Sci. (2011).
- [41] A. Doshi, S. Channiwala, P. Singh, Inlet impeller rounding in pumps as turbines: an experimental study to investigate the relative effects of blade and shroud rounding, Exp. Therm. Fluid Sci. (2017).
- [42] P. Singh, J.T. Kshirsagar, S. Caglar, F. Nestmann, Natanasabapathi, Experimental and computational studies of the effect of 'casing eye rib' on the swirl flow at the exit of a pump as turbine, in: Proceedings of the ASME Heat Transfer/Fluids Engineering Summer Conference 2004, HT/FED 2004, 2004.
- [43] P. Singh, Optimization of Internal Hydraulics and of System Design for PUMPS AS TURBINES with Field Implementation, PhD thesis, Institut für Wasserwirtschaft und Kulturtechnik, Universität Karlsruhe (TH), 2005.
- [44] Y. Sun-Sheng, K. Fan-Yu, F. Jian-Hui, X. Ling, Numerical research on effects of splitter blades to the influence of pump as turbine, Int. J. Rotating Mach. (2012).
- [45] T. Capurso, L. Bergamini, M. Torresi, Design and cfd performance analysis of a novel impeller for double suction centrifugal pumps, Nucl. Eng. Des. 341 (2019) 155–166.
- [46] T. Capurso, L. Bergamini, S.M. Camporeale, B. Fortunato, M. Torresi, Cfd analysis of the performance of a novel impeller for a double suction centrifugal pump working as a turbine, in: 13 Th European Conference On Turbo-machinery Fluid Dynamics & Thermodynamics, EUROPEAN TURBOMACHINERY SOCIETY, 2019.
- [47] S.S. Yang, H.L. Liu, F.Y. Kong, B. Xia, L.W. Tan, Effects of the radial gap between impeller tips and volute tongue influencing the performance and pressure pulsations of pump as turbine, J. Fluid Eng.Trans. ASME (2014).
- [48] H.A. Arani, M. Fathi, M. Raisee, S.A. Nourbakhsh, A novel volute design for reducing radial force in pump and PAT, in: IOP Conference Series: Earth And Environmental Science, 2019.
- [49] H. Alemi Arani, M. Fathi, M. Raisee, S.A. Nourbakhsh, The effect of tongue geometry on pump performance in reverse mode: an experimental study, Renew. Energy (2019).
- [50] D. Štefan, M. Rossi, M. Hudec, P. Rudolf, A. Nigro, M. Renzi, Study of the internal flow field in a pump-as-turbine (pat): numerical investigation, overall performance prediction model and velocity vector analysis, Renew. Energy (2020).
- [51] J.F. Gulich, Centrifugal Pumps, 2 ed., Springer, 2010.
- [52] NUMECA International, AutoGridsTM 13.2, 2019. <https://www.numeca.com>.
- [53] NUMECA International, HexpressTM 8.1, 2019. <https://www.numeca.com>.
- [54] NUMECA International, HexpressViewTM 8.1, 2019. <https://www.numeca.com>.
- [55] A. Morabito, G. de Oliveira e Silva, P. Hendrick, Deriaz pump-turbine for pumped hydro energy storage and micro applications, J. Energy Storage (2019).
- [56] NUMECA International, FINE/Open 8.1. <https://www.numeca.com>, 2019.
- [57] A. Corsini, G. Delibra, A.G. Sheard, A critical review of computational methods and their application in industrial fan design, International Scholarly Research Notices (2013) 2013.
- [58] R.N. Pinto, A. Afzal, L.V. D'Souza, Z. Ansari, A.M. Samee, Computational fluid dynamics in turbomachinery: a review of state of the art, Arch. Comput. Methods Eng. 24 (3) (2017) 467–479.
- [59] J.D. Denton, Some limitations of turbomachinery cfd, in *Turbo Expo: Power for Land, Sea, and Air* 44021 (2010) 735–745.
- [60] T. Capurso, M. Stefanizzi, G. Pascazio, S. Ranaldo, S.M. Camporeale, B. Fortunato, M. Torresi, Slip factor correction in 1-D Performance prediction model for PATs, Water (Switzerland) (2019).
- [61] J.E. Bardina, P.G. Huang, T.J. Coakley, Turbulence modeling validation, testing, and development, NASA Tech. Memorand. (1997).
- [62] A. Morabito, P. Hendrick, Pump as turbine applied to micro energy storage and smart water grids: a case study, Appl. Energy 241 (2019) 567–579.
- [63] R.H. Dieck, Measurement uncertainty models, ISA (Instrum. Soc. Am.) Trans. 36 (1) (1997) 29–35.
- [64] R.B. Abernethy, R.P. Benedict, R.B. Dowdell, ASME measurement uncertainty, J. Fluid Eng. 107 (06 1985) 161–164.
- [65] J.H. Friedman, Multivariate adaptive regression splines, Ann. Stat. (1991) 1–67.
- [66] M. Kuhn, K. Johnson, et al., Applied Predictive Modeling, vol. 26, Springer, 2013.
- [67] J. Rudy, Package Sklearn-Contrib-Py-Earth Version 0.1.0, 2013. <https://contrib.scikit-learn.org/py-earth/index.html>.
- [68] G.H. Golub, M. Heath, G. Wahba, Generalized cross-validation as a method for choosing a good ridge parameter, Technometrics 21 (2) (1979) 215–223.
- [69] Mathworks, Matlab Version 9.1. (R2016b), Natick, Massachusetts vol. 698, 2016.
- [70] F.J. Hickernell, Y.-x. Yuan, A Simple Multistart Algorithm for Global Optimization, 1997.
- [71] W. Tu, R. Mayne, Studies of multi-start clustering for global optimization, Int. J. Numer. Methods Eng. 53 (9) (2002) 2239–2252.
- [72] S. Derakhshan, A. Nourbakhsh, Theoretical, numerical and experimental investigation of centrifugal pumps in reverse operation, Exp. Therm. Fluid Sci. (2008).
- [73] T. Mercier, C. Hardy, P. Van Tichelen, M. Olivier, E. De Jaeger, Control of variable-speed pumps used as turbines for flexible grid-connected power generation, Elec. Power Syst. Res. 176 (2019) 105962.
- [74] A. Morabito, G. Furtado, A. Amarante Mesquita, P. Hendrick, Variable speed

- regulation for pump as turbine in a micro pumped hydro energy storage application, in: Proceedings of the 38th IAHR World Congress—“Water: Connecting the World”, Panama City, Panama, 2019, pp. 1–6.
- [75] M. Tahani, A. Kandi, M. Moghimi, S.D. Houreh, Rotational speed variation assessment of centrifugal pump-as-turbine as an energy utilization device under water distribution network condition, *Energy* 213 (2020) 118502.
- [76] C.E. Brennen, *Hydrodynamics of Pumps*, 1 ed., Concepts ETI, Inc., 1994.
- [77] J.-M. Chapallaz, P. Eichenberger, G. Fischer, *Manual on Pumps Used as Turbines*, 1992. No. BOOK, Vieweg Braunschweig, Germany.
- [78] A. Morabito, Experimental and numerical analysis of a pump as turbine in micro pumped hydro energy storage, PhD Thesis, Université libre de Bruxelles, Brussels, 2021.